IEEE Access
Multidisciplinary | Rapid Review | Open Access Journal

Received 21 December 2020, accepted 29 December 2020, date of publication 8 January 2021, date of current version 20 January 2021.

Digital Object Identifier 10.1109/ACCESS.2021.3050201

Non-Uniform Narrow Groove Plasmonic Nano-Gratings for SPR Sensing and Imaging

AJAY KUMAR AGRAWAL, AAKANSHA SUCHITTA, AND ANUJ DHAWAN, (Member, IEEE)
Electrical Engineering Department, IIT Delhi, New Delhi 110016, India

Corresponding author: Anuj Dhawan (adhawan@ee.iitd.ac.in)

This work was supported in part by the Ministry of Human Resource Development (MHRD) through the UAY Program under Grant RP03246G and the IMPRINT Program under Grant RP03417G; in part by the Science and Engineering Research Board (SERB) under Grant RP03055G; in part by the Department of Biotechnology, Ministry of Science and Technology (DBT), under Grant RP03150G; and in part by the Defense Research and Development Organization (DRDO) under Grant RP03356G and Grant RP03436G.

ABSTRACT A surface plasmon resonance sensing and imaging platform based on plasmonic non-uniform nano-gratings with narrow groove (sub-10 nm) is presented. In these nanogratings, normally incident optical radiation is directly coupled to surface plasmons without the requirements of any other conventional surface plasmon coupling mechanisms such as prism-based or grating-based coupling. Theoretical analysis of practically realizable plasmonic non-uniform nano-gratings with rounded tops and slanted sidewalls is carried out to numerically to determine reflectance and differential reflectance signals when the localized refractive index of the medium around the gold layer present in these nano-gratings is changed. This change in the localized refractive index can occur due to the binding of biomolecules to the gold layer. Two kinds of plasmonic non-uniform nano-gratings are studied using finite difference time domain (FDTD) modelling: gold nano-gratings (GNGs) and gold-coated silicon nano-gratings (GSNGs). The plasmonic non-uniform nano-gratings being proposed, more specifically the GSNGs, can be easily fabricated with the presently existing nanofabrication and thin film deposition methods as opposed to uniform nano-gratings (with parallel sidewalls) that are very difficult to fabricate. The plasmonic non-uniform nano-gratings with narrow grooves eliminate the strict requirements on the angle of incidence for coupling of light into surface plasmons, which are needed in conventional prism-based coupling mechanisms. By employing FDTD calculations, we demonstrate that these plasmonic non-uniform nano-gratings provide very high differential reflectance amplitude values, which are indicative of high sensitivities of the SPR or SPRi sensors when the localized refractive index around the sensors is varied. Moreover, the sensors being proposed in this article provide a maximum sensitivity of localized refractive index sensing (i.e. surface sensitivity or S_S) of 70 nm/nm with a figure of merit of the localized sensor (FOM_S) of 1.5 nm^{-1}. This sensitivity of localized refractive index sensing is the highest reported thus far in comparison with previously reported plasmonic sensors. Moreover, these plasmonic non-uniform nano-grating based sensors exhibit significantly better performance when compared with conventional SPR or SPRi sensors based on the Kretschmann configuration.

INDEX TERMS FDTD, localized sensing, nano-gratings, SPR imaging, SPR sensors, surface plasmon.

I. INTRODUCTION

Surface plasmons are collective oscillations of conduction electrons at the interface of a metal and a dielectric [1]–[7]. When the surface plasmons are coupled to the incident electromagnetic (EM) fields, they are called surface plasmon polaritons (SPPs). For SPPs propagating on metal-dielectric interfaces, substantial EM field enhancements are observed at the interfaces. When light is coupled to SPPs propagating on such interfaces, sharp dips in the spectra of the reflected light are observed at certain resonant wavelengths, these resonances being termed as the surface plasmon resonances (SPRs). The propagating surface plasmon polaritons can be present in a single metal-dielectric interface, in multiple metal-dielectric interfaces (such as those in plasmonic waveguides), as well as in a plasmonic nano-gratings. On the other hand, localized surface plasmons (LSPs) describe oscillations of conduction electrons at the surface of bounded

The associate editor coordinating the review of this manuscript and approving it for publication was Yee Sin Ang.

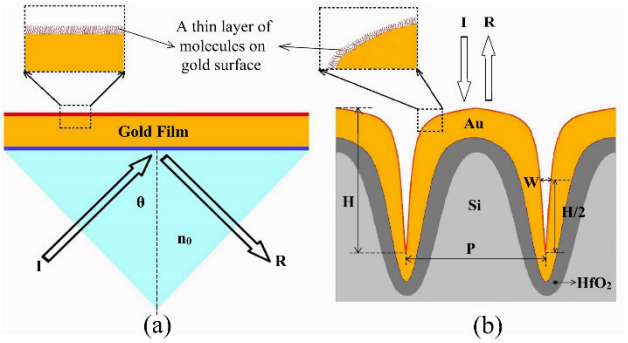

FIGURE 1. (a) The Kretschmann configuration for a 40 nm gold film. (b) A schematic showing a cross-sectional view of non-uniform gold-coated silicon nano-gratings (GSNG).

geometries of metal-dielectric interfaces, such as metallic nanoparticles or nanostructures. Upon excitation of LSPs in nanoparticles of plasmonics-active metals (such as gold, silver, or copper), peaks in the scattering and absorption spectra associated with these nanoparticles are observed at certain resonant wavelengths in the visible or near-IR spectral regimes. Excitation of LSPs (at certain resonant wavelengths) leads to a substantial EM field enhancement in the near vicinity of the nanoparticles [8]–[13]. These EM fields rapidly decay away from the nanoparticle-dielectric boundaries.

The enhancement of EM fields in the vicinity of the metal-dielectric interfaces results in extremely high sensitivity of the propagating SPPs and the LSPs to changes in surface conditions at the metal-dielectric interfaces. Hence, propagating SPPs and the LSPs are employed for sensing refractive index (RI) changes of the dielectric medium or layer in the vicinity of the metallic surface. Therefore, they are extensively used for the development of chemical and biological sensors [14]–[17]. SPPs and LSPs are also employed in plasmonics-enhanced solar cells [18] and optical switching and modulation [19]. Moreover, there are several photonic phenomena that employ the excitation of propagating SPPs and LSPs such as surface-enhanced Raman scattering (SERS) [20]–[24], plasmon-enhanced fluorescence (PEF) [25], non-linear optics [26].

Conventional Surface plasmon resonance (SPR) chemical and biological sensors are primarily based on either prism-coupling configurations (Kretschmann or Otto) or on grating-based coupling [27], [28] to couple the incident optical radiation to propagating SPPs. There has been extensive research in employing spectral and angular interrogation based thin-film SPR sensors (using the Kretschmann configuration — See Fig. 1(a)) for detecting localized or bulk changes in refractive indices. The past decade has seen a surge of interest in surface plasmon resonance imaging (SPRi) technique, which has emerged as a favorable method for investigating label-free biomolecular interactions, molecular binding events in target molecules or kinetic processes [29]–[32]. SPR sensors carry out detection of reflectivity changes caused by perturbations resulting from molecular interactions or binding events or any other biochemical reactions that occur at plasmonics-active metal surfaces, which induce deviations in resonant conditions. In SPR imaging (SPRi), such changes in the reflectance spectra are efficiently captured by using a CMOS/CCD camera in the form of movies that capture the images of the spatial maps of the SPR sensor chips (having the biomolecules localized at different locations on the sensor chip) for different wavelengths of the incident radiation.

The current biomedical research requires detection of antigens present at extremely low concentrations of target analytes and at the same time distinguishing between various molecules in the biomaterial. There are several diagnostic platforms, such as enzyme-linked immune sorbent assays (ELISA), radio-immunoassays, or fluorescence-based assays. However, SPR and LSPR diagnostic techniques have dominated the current state-of-the-art technology for providing highly reliable and sensitive detection of analytes with enhanced specificity. These label-free techniques are being extensively employed by researchers working in the field of biosensors due to their distinct advantage over the conventional labelling assays, as a label may damage or altogether modify the chemical structure of the molecular affinity binding electrons. SPR is prevalently used in the detection of genetically engineered organisms and cellular mutations and in monitoring DNA hybridizations. It is also predominantly employed in the study of several biochemical binding events such as DNA-DNA, DNA-protein, protein-protein or antigen-antibody interactions, in which analyte molecules modulate the properties of light reflected from a nanoscale plasmonic thin film or nanostructured plasmonic geometries (such as nanohole arrays in plasmonic thin films). The reflected or transmitted (in the case of nanohole arrays) light from such plasmonic structures carry sufficient information to obtain knowledge of such biochemical phenomena, which can be deciphered from spectral and angular distributions of reflectance and transmittance as well as changes in intensities or states of polarization. LSPR based detection regimes, on the other hand, concentrate on detecting the localized RI changes around plasmonic nanoparticles in solution or plasmonic nanostructures on substrates or chips. These localized variations in RI may result from the attachment of analyte molecules to the surface of the plasmonic nanoparticles or substrates.

Plasmonic nano-gratings have been investigated for several applications such as for molecular biosensing in a label-free fashion [33], fluorescence imaging of live cells using nano-grating based enhancement [34] and in non-linear optics [26], [35], [36]. There are several types of plasmonic modes that can be present in nano-grating structures. The first set of modes are propagating SPP modes, which are characterized by the presence of dominant EM fields at the top surface of the nanogratings and weaker fields in the groove widths. The second set of modes are the plasmonic waveguide modes [37]–[43], which are characterized by the EM fields localized inside the grooves of the nano-gratings. Another set of

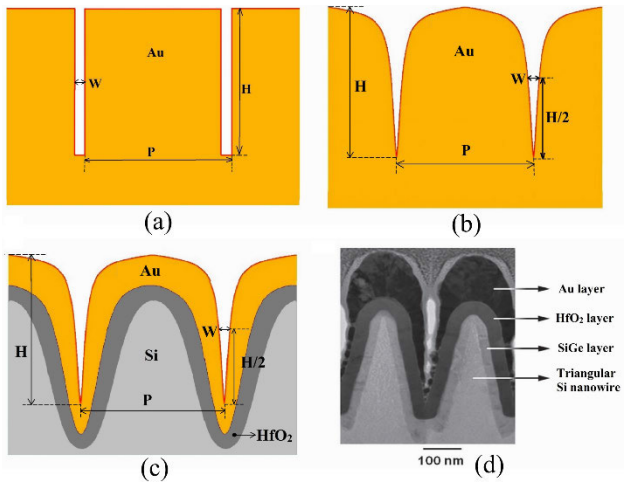

FIGURE 2. Schematic diagrams illustrating different types of nano-gratings: (a) uniform rectangular aperture nano-gratings, (b) non-uniform gold nano-gratings (GNGs), and (c) gold-coated silicon nano-gratings (GSNGs). 'H' and 'P' represent the height and periodicity of the nanogratings, respectively. The groove width is denoted by 'W' and is calculated at a height 'H/2' from the bottom of the nano-grating. (d) SEM/TEM cross-section of gold-coated silicon nano-gratings over-coated with hafnium oxide (HfO2) layer for smooth deposition of metallic gold film and reducing gaps between adjacent silicon nano-grating structures [45].

modes are the hybridized modes that comprise of both the propagating SPP modes and the plasmonic waveguide modes localized in nanograting grooves.

The plasmonic non-uniform nanograting proposed in this article have narrow grooves in the sub-wavelength regime (with sub-10 nm groove widths or gaps present in the nano-gratings). In these nanostructures, surface waves on the opposite plasmonic surfaces of the groove couple resulting in plasmonic waveguide modes. These plasmonic waveguide modes are confined inside the nanograting grooves, which are characterized by considerable enhancement of EM fields inside the grooves [44]. The analyte molecules being sensed (whose binding causes localized RI changes in the narrow groove plasmonic nano-gratings) will be present in these high EM field regions lying inside the narrow grooves. Hence, very high sensitivity — and therefore high values of the differential reflectance — of detection of these molecules is expected (see Fig. 1(b)). Moreover, for these nano-gratings we observe multiple plasmonic dips in reflectance spectra, which can enable carrying out SPR sensing at multiple wavelengths. The sensors being proposed in this article provide a maximum sensitivity of localized refractive index sensing (i.e. surface sensitivity or S_S) of 70 nm/nm with a figure of merit of the localized sensor (FOM_S) of 1.5 nm^{-1}. This sensitivity of localized refractive index sensing is the highest reported thus far in comparison with previously reported plasmonic sensors.

In this article, we present FDTD simulation results showing the optical characteristics of two kinds of plasmonic non-uniform nano-gratings: (a) gold nano-gratings (GNGs) (see Fig. 2(b)) and (b) gold-coated silicon nano-gratings (GSNGs) (see Fig. 2(c-d)), and compare the results with uniform rectangular aperture nano-gratings (see Fig. 2(a)) and the conventional SPR-based prism coupling systems. The term 'non-uniform' is being used to describe practical and realizable nano-grating structures with non-parallel slanted sidewalls and rounded tops. The numerical analysis is based on differential reflectance (DR) calculations for the narrow-groove plasmonic nano-gratings for different geometrical parameters of these nano-gratings.

While the fabrication of the ideal rectangular aperture based nano-grating structures (i.e. narrow-groove nano-gratings having parallel side-walls) can be very difficult, the proposed non-uniform nano-gratings can be easily fabricated using the conventional nanofabrication processes (described at the end of this section). The non-uniform nano-grating structures presented in this work are almost as good as those reported previously by Wang *et al.* [45] in terms of achieving substantially high values of differential reflectance (DR) signals. The high DR signals are indicative of high sensitivity of the SPR or SPRi sensors for a change in the refractive index.

Moreover, the proposed plasmonic non-uniform nano-gratings have numerous advantages compared to the conventional prism coupling based SPR sensors as these nano-grating sensors are based on direct coupling of light into plasmonic modes — there is no requirement of any prism coupling mechanism to couple light into surface plasmons and even normally incident light can be coupled to the plasmonic modes. The proposed plasmonic nano-grating structures also offer the possibility of carrying out SPR sensing at several wavelengths (employing LEDs/laser diodes of different wavelengths) as the reflectance spectra of these nano-gratings exhibit several plasmon resonance-related dips (occurring at multiple wavelengths) in different regimes such as visible or near-IR. Additionally, since no coupling mechanism is required to couple incident light into surface plasmons, design of miniaturized SPR sensors employing these non-uniform nano-gratings is possible. In addition, the previously reported work on narrow-groove nano-gratings [45] is primarily based on SERS based reflectance spectra calculation using Rigorous Coupled Wave Analysis (RCWA), whereas we have presented Finite Difference Time Domain (FDTD) calculations to determine the reflectance spectra associated with these non-uniform nano-gratings.

The latest developments in nanofabrication methodologies have enabled researchers to fabricate complex nanostructures with even sub-10 nm gap structures. The non-uniform gold-coated silicon nano-gratings (GSNGs) can be fabricated easily by using a combination of conventional lithography and deposition techniques. 193 nm deep-UV lithography can be employed using an ASML 5500/950B scanner to fabricate a 1-D silicon nano-gratings. This can be followed by growth of a layer of silicon germanium using rapid thermal CVD as an optional step to make the gap between adjacent pillars of silicon nano-grating narrower. The distance between the walls of adjacent grooves of the nanogratings can be

further reduced by depositing a conformal layer of hafnium oxide or platinum on these nanowires using atomic layer deposition (ALD). Subsequently, a plasmonic metal can be deposited to over-coat these 1-D 'non-uniform nano-gratings' [45]. Fig. 2(d) shows TEM cross-section of previously fabricated non-uniform nanogratings [45]. Our calculations based on FDTD simulations are expected to provide accurate modelling of practically realizable plasmonic narrow-groove nano-gratings. The nano-gratings modelled in our work can be employed for reliable and sensitive detection of localized fluctuations in refractive index resulting from biomolecular interactions of target analytes with the nano-grating metallic surface, making these structures an ideal platform for SPR and SPRi based sensing.

II. NUMERICAL MODELLING USING FDTD AND RCWA

The proposed non-uniform plasmonic nano-grating structures are studied theoretically by employing Finite-Difference Time-Domain (FDTD) modelling. These nano-grating structures were simulated for determining differential reflectance — before and after localized refractive index variations on nano-grating surfaces — using FDTD modelling. FDTD modelling technique [3], [5], is an analytical method in computational electrodynamics [46] for solving the differential form of coupled Maxwell's equations. The finite-difference time domain method solves discretized Maxwell's equations updating electric field vectors from magnetic field vectors and vice-versa until stabilized electromagnetic field behavior is developed. This is done by staggering both vector components in space and time. In our work, a commercial FDTD software called FDTD solutions (from Lumerical Solutions) was employed. This FDTD software incorporates dispersion models such as Drude, Lorentz-Drude, and Debye models. In our simulations, the relative permittivity of gold was modelled using Lorentz-Drude dispersion model from literature [47]. The polarization of incident plane wave radiation was taken as TM polarization, in all the FDTD simulations employed for determining the reflectance spectra for the proposed nano-gratings. In our simulations, the plane wave radiation was normally incident on the nano-gratings (see Fig. 1(b)) for different wavelengths of the incident light.

FDTD simulations were employed for studying the changes in the reflectance spectra for the GNGs and GSNGs due to localized RI changes on the nano-grating surface — such as those caused by the adsorption or binding of biomolecules on the nano-grating surface. When biomolecules adsorb on the gold nanograting surface, the refractive index of the region just above (thickness of this region being $\sim$ 2 nm) the gold nano-grating surface is expected to change from 1.33 (refractive index of water or aqueous buffer solution) to $\sim$ 1.53 [38]. Hence, the biomolecule layer present on the nanograting surface was simulated by placing a 2 nm thick layer of a material having RI of 1.53 on nanograting surface. The region above the 2 nm biomolecule layer was assumed to have a uniform refractive index of 1.33 (water or aqueous buffer solution). In our FDTD simulations, several geometrical parameters of the GNG and GSNG grating structures — such as periodicity, width, and height — were varied to study their effects on the differential reflectance (DR). It has to be noted that differential reflectance quantifies the effect of varying in the localized RI around the nanograting surface — a high value of the differential reflectance indicates a high sensitivity of localized refractive index sensing based on the SPR or SPRi sensors.

FDTD simulations were employed for determining the reflectance spectra for the GNGs and GSNGs. In these FDTD simulations, 2-D solutions of the electromagnetic fields were obtained for the proposed GNGs and GSNGs. A plane wave optical radiation — with wavelengths ranging from 600 nm to 1500 nm — was normally incident on the gratings. The mesh parameters and time steps (Δt) were appropriately chosen so that the Courant stability criterion [46] was satisfied. In our FDTD simulations, we have taken 64 perfectly matched layers (PML) and a mesh accuracy of 5 (i.e. 22 number of cells per wavelength). Convergence studies for certain critical parameters — such as the mesh size, number of PML layers, mesh accuracy, and the distance of the PML layers from the nanostructures — were carried out to ensure the accuracy of our FDTD simulations. In each convergence study, we varied one parameter (the parameter being optimized) keeping the other parameters to be constant till the results (Reflectance Amplitude (DR_{AMP}) and wavelength shift ($\Delta\lambda$) values) stopped changing. We firstly achieved the convergence of the distance of the PML layers from the nanostructures keeping the mesh size to 1 nm, number of PML layers to be 12, and mesh accuracy to be 5. After the convergence tests, the distance of the PML layers from the nanostructures was calculated to be 500 nm. Then the convergence study for the number of PML layers was carried out and the optimal value of number of PML layers was calculated to be 64 layers. Keeping the perfectly matched layer (PML) to be at a distance of 500 nm from the nanostructures and a total 64 layers to minimise the reflections from boundary, we carried out the convergence studies for mesh accuracy taking the mesh size to be 1 nm. The mesh accuracy was optimized to 5. Finally, taking the mesh accuracy to be 5, distance of the PML layers from the nanostructures to be 500 nm, and number of PML layers to be 64 layers, mesh size convergence studies were carried out. In the non-uniform nano-gratings being proposed in this article, the minimum feature size is that of the biomolecule layer (i.e. the layer formed by the adsorption or binding of biomolecules on the surface of the plasmonic metal), which was taken to be 2 nm. Accordingly, for the GNGs and GSNGs, the mesh sizes were selected to be 0.4 nm in all directions (Δx, Δy, and Δz) as convergence in the values of the Differential Reflectance Amplitude (DR_{AMP}) and wavelength shift ($\Delta\lambda$) was obtained for values below a mesh size of 0.6 nm. The initial results were optimized for single wavelength and then compared with the broadband source for any error measurements.

The differential reflectance spectrum for a continuous gold film deposited on a glass prism (i.e. for the Kretschmann configuration) was calculated using Rigorous Coupled Wave Analysis (RCWA), which is a semi-analytical technique in computational electrodynamics [48]–[50]. In these simulations, light (of wavelengths varying between 600 nm to 1500 nm) was incident on a 40 nm thick layer of gold film at an angle 'θ' (which was varied from 55° to 90°). The gold film layer was present on a glass substrate (the glass substrate represents a BK7 glass prism) having a refractive index of 1.5142, with a 1 nm adhesion layer of titanium being present in between the gold layer and the glass substrate (see Fig. 1(a)). The presence of a biomolecule layer on the surface of the gold film was simulated by placing a 2 nm thick layer of a material having a refractive index of 1.53 [38] on the gold film surface. The refractive index of the region above the biomolecule layer was taken to be 1.33 (aqueous media). In RCWA, the spatial dependence of a harmonic electromagnetic field in a periodic structure is represented as a linear combination of spatial harmonics [48], [49]. In our work, a commercial RCWA software called DiffractMOD (from Synopsis Optical Solutions Group) was employed. In our RCWA simulations, convergence studies were carried out for the number of harmonics till the results (Reflectance Amplitude (DR_{AMP}) and wavelength shift ($\Delta\lambda$) values) stopped changing. For these RCWA simulations, the simulation accuracy has been achieved by selecting five harmonics.

III. RESULTS AND DISCUSSION

The non-uniform narrow groove nano-grating based SPR and SPRi sensing platforms being proposed are significantly different from the previously reported platforms based on uniform rectangular aperture nano-gratings [38] or the conventional prism coupling based SPR and SPRi sensors [28]. In this article, we present two non-uniform nano-grating configurations, namely, gold nano-gratings and gold-coated silicon nano-gratings. The former are nano-gratings made only of gold and having a non-uniform geometry, i.e. having slanted sidewalls and rounded tops (see Fig. 2(b)). The latter configuration consists of a gold coating on a thin conformal layer of HfO_2, which is deposited on silicon nano-gratings (see Fig. 2(c-d)). Binding or adsorption of the biomolecules on the surface of the nanogratings leads to localized RI changes at the metal-dielectric interface. These binding events could be antigen-antibody, DNA-DNA, DNA-protein, or protein-protein interactions. Through numerical simulations, we demonstrate the applicability of these non-uniform narrow groove nano-gratings for highly sensitive detection of localized changes of refractive index at the nano-grating surface. The schematics of the conventional rectangular aperture nano-gratings and the non-uniform nano-gratings are shown in Fig. 2(a-c). Dhawan *et al.* [45] have previously fabricated the non-uniform nano-gratings with rounded tops and slanted sidewalls. The TEM cross-section of this structure is shown in Fig. 2(d).

We first compared the simulation results of the non-uniform narrow groove nano-gratings (see Fig. 3(b-c)) with those of a continuous plasmonic thin film employing the Kretschmann configuration (see Fig. 3(a)). Fig. 3(a) shows a differential reflectance (DR) spectra obtained using RCWA simulations for a continuous plasmonic thin film employing the Kretschmann configuration. It was observed that when the wavelength of the incident radiation was scanned (spectral scanning) from 600 nm to 1500 nm (taking the incidence angle of light to be 64°), the minimum and maximum values of DR were determined to be −0.1040 and 0.1726, respectively. Hence, the maximum differential reflectance amplitude (DR_{AMP}), i.e. the absolute distance between the peak and bottom values of the DR spectrum, was calculated to be 0.2766. The reflectance and DR spectra for the non-uniform GNGs for normal incidence of light are shown in Fig. 3(b). We observe plasmonic dips at multiple wavelengths corresponding to multiple waveguide modes confined into the narrow grooves of the grating. This is due to the large height (H = 200 nm) of the GNGs as light is coupled into several waveguide modes inside narrow grooves of the nanogratings. Moreover, we observe a large red-shift of the resonance wavelength in the reflectance spectrum for these gratings when the localized refractive index above the nano-grating surface was varied from 1.33 (see green curve in Fig. 3(b)) to 1.53 (see red curve in Fig. 3(b)). At plasmon resonance wavelengths, extremely high electromagnetic (EM) fields are confined inside the grooves of the nanogratings. Hence, a localized change in the RI occurring inside the nano-grating grooves (in the regions of high EM fields) leads to a large red-shift of plasmon resonance wavelengths in the reflectance spectrum. The differential reflectance amplitude (DR_{AMP}) for this structure was calculated to be 0.9794 (See Fig. 3(b)), which is substantially higher compared to the DR_{AMP} obtained for a 40 nm plain gold film employing the Kretschmann configuration. The large value of DR_{AMP} results from the large red-shift in the reflectance spectrum when the localized RI above the surface of the gratings was varied from 1.33 to 1.53. In the case of GSNGs also, we observe plasmonic dips at multiple wavelengths corresponding to multiple waveguide modes inside the nanograting grooves (see Fig. 3(c)). This is due to the large height (H = 200 nm) of the GSNGs as light is coupled into several waveguide modes confined into the narrow nanograting grooves.

We primarily employ differential reflectance (DR) to quantify the changes in spectra after binding of a 2 nm layer of biomolecules to the surface of GNGs and GSNGs instead of detecting the change in the position of plasmon resonance wavelengths ($\Delta\lambda$). This is because in a practical scenario, it is difficult to measure $\Delta\lambda$ as this first requires accurate determination of the positions of the plasmon resonance dips (by calculating the spectral position where the slope of the reflectance spectra is zero). The measurements of shifts in the position of the wavelengths of plasmon resonance become very difficult for a very small values of $\Delta\lambda$. In contrast, calculation of the difference between the spectra obtained

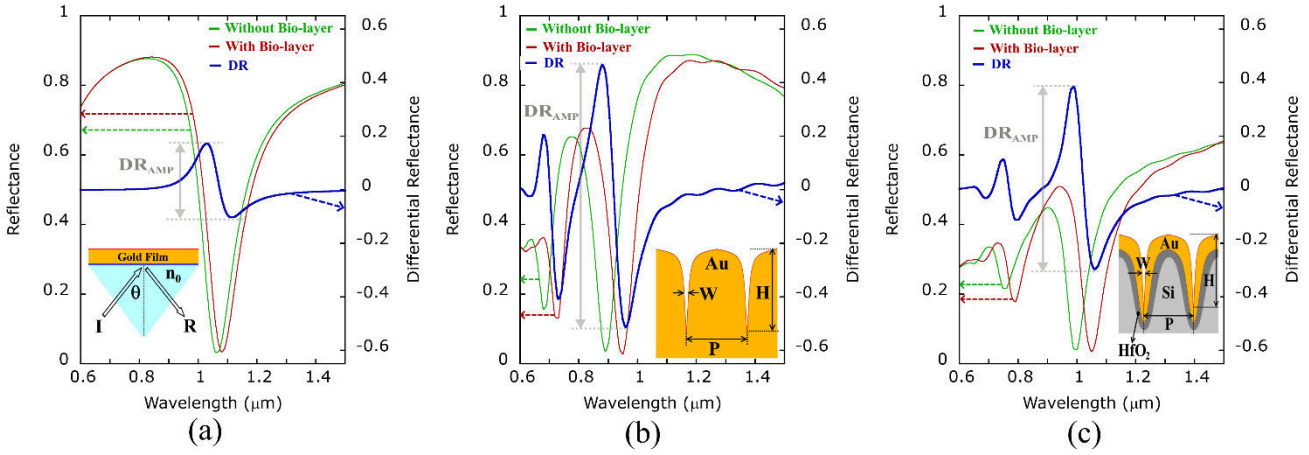

FIGURE 3. (a) RCWA simulations of a 40 nm thick continuous gold film employing the Kretschmann configuration, (b) Results of FDTD simulations for GNGs, and (c) Results of FDTD simulations for GSNGs showing the reflectance spectra and differential reflectance spectra. Geometrical parameters for the non-uniform nanogratings are periodicity 'P' = 200 nm, height 'H' = 200 nm, and groove width 'W' = 16.5 nm.

before and after biomolecular binding on the surface of the GNGs and GSNGs is easy and quantification of the DR can be carried out by calculating either the peak DR or the DR amplitude (as described in Fig. 3). Furthermore, DR calculation is also suitable for SPR imaging as the difference of reflectance images (spatial reflectance maps) can be taken for the cases after and before the binding of the biomolecules on the nanograting surface.

Normally incident optical radiation is coupled into plasmonic waveguide modes in the proposed non-uniform nanogratings, which results in standing waves localized inside the grooves. This leads to strong EM fields being present inside the narrow grooves of these gratings. The spatial distribution of E-field enhancement (i.e. $|E| / |E_0|$), where $|E|$ represents the magnitude of E-field around the gold nanogratings and $|E_0|$ represents the magnitude of the incident E-field) in non-uniform GNGs are shown in Fig. 4(a-b) for off-resonance and on-resonance conditions, respectively. At a wavelength of 950 nm (on-resonance, i.e. plasmon resonance associated with a plasmonic waveguide mode coupled into the nanogratings), there is a significant enhancement in the EM fields inside the narrow nanograting grooves as compared to the case when the structure is illuminated with a wavelength of 1180 nm (off-resonance wavelength). In the case of GSNGs, it was observed that the on-resonance wavelength is 1090 nm, and the off-resonance wavelength is 1500 nm (see Fig. 4(c-d)). These plasmon resonance wavelengths are red-shifted in the case of GSNGs when compared with the spectra of GNGs. Light is effectively coupled into plasmonic waveguide modes for all-gold (GNGs) nano-gratings (whose unit cell resembles an MIM plasmonic waveguide structure. In contrast, the EM fields are not entirely confined inside the narrow grooves for GSNGs (whose unit cell resembles an IMIMI plasmonic waveguide structure). This is because the electromagnetic fields also exist in the outer insulator regions (HFO_2) of the IMIMI

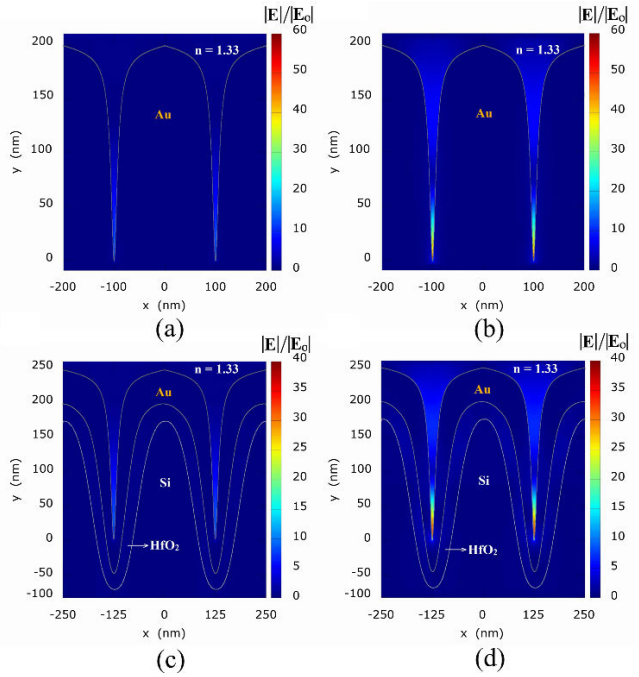

FIGURE 4. FDTD simulation results showing the spatial distribution of E-field enhancement ($|E| / |E_0|$,) in non-uniform gold nano-gratings for an excitation wavelength of (a) 1180 nm (off-resonance) and (b) 950 nm (on-resonance). Geometrical parameters for these non-uniform gold nano-gratings are periodicity 'P' = 200 nm, height 'H' = 200 nm, and groove width 'W' = 16.5 nm. FDTD simulation results showing the spatial distribution of E-field enhancement in non-uniform gold-coated silicon nano-gratings for an excitation wavelength of (c) 1500 nm (off-resonance) and (d) 1090 nm (on-resonance). The geometrical parameters for these non-uniform nano-gratings are periodicity 'P' = 250 nm, height 'H' = 200 nm, and groove width 'W' = 20.625 nm.

waveguide-like structure which has a higher refractive index as compared to the central insulator region (water or aqueous buffer solution) which is also shown in Figs. 4 (c)-(d). This explains the red-shift of the reflectance spectra in the case of the GSNGs as compared to the GNGs.

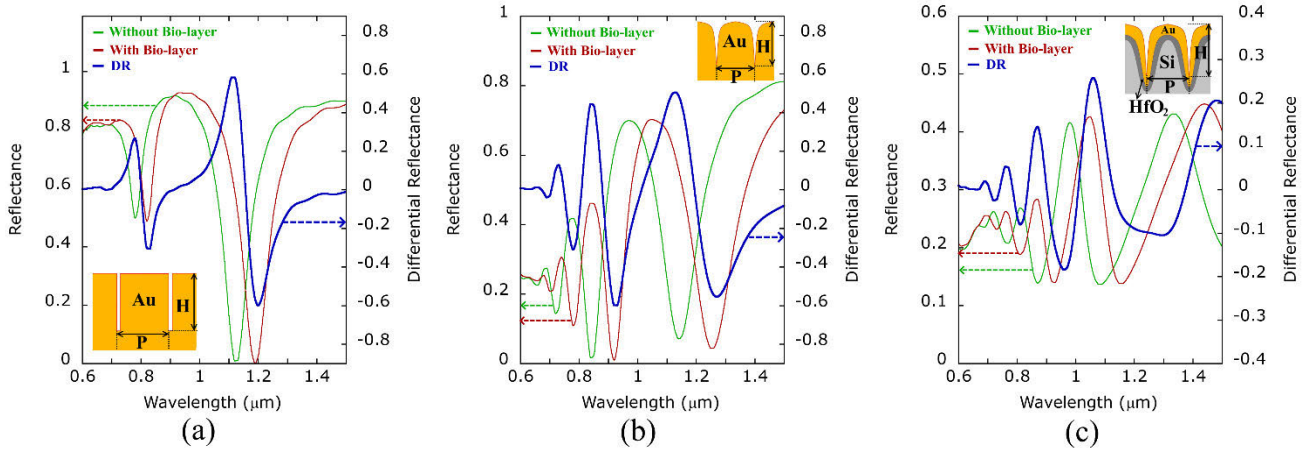

FIGURE 5. FDTD simulation results showing reflectance spectra and DR spectra for: (a) uniform rectangular aperture gold nano-gratings, (b) non-uniform gold nano-gratings (GNGs), and (c) non-uniform gold-coated silicon nano-gratings (GSNGs). The geometrical parameters for these nano-gratings are periodicity 'P' = 100 nm, height 'H' = 200 nm, and groove width 'W' = 8.25 nm.

A comparison of the non-uniform nano-gratings being proposed and the previously reported rectangular aperture uniform nano-gratings was carried out by calculating the reflectance spectra and the DR spectra, and the results are shown in Fig. 5. It was observed that for the same spectral window of 600 nm to 1500 nm and for the same geometrical considerations, there was an increase in the number of plasmon modes in the reflectance spectra for the proposed non-uniform nanogratings. This is attributed to light being coupled into a larger number of plasmonic waveguide modes in the non-uniform nanogratings when compared with the rectangular aperture uniform nano-gratings. This is due to the fact that, in the case of non-uniform nanogratings, the groove width changes with height and as a result, several groove widths are present. This results in light being coupled into multiple plasmonic waveguide modes in the non-uniform GNGs and GSNGs, with the different modes corresponding to the different groove-widths in the non-uniform GNGs and GSNGs. Moreover, we observed that in the case of GNGs and GSNGs, the reflectance spectra showed a broadening of the plasmon resonance-related dips. In these nano-gratings, several groove widths are present which results in the superposition of the reflectance spectra corresponding to the different groove widths, and therefore the broadening of the dips in the reflectance spectra.

It can also be observed from Fig. 5 that the differential reflectance amplitude (DR_{AMP}) values for the non-uniform nano-gratings are lower than those for the ideal rectangular aperture nano-gratings. The DR_{AMP} for the rectangular aperture nano-gratings, the non-uniform GNGs, and the non-uniform GSNGs were calculated to be 1.1821, 1.0602, and 0.3629, respectively. There is a broadening of dips in the reflectance spectra for the non-uniform nanogratings (as explained above), which results in a reduction in the values of DR_{AMP}. Hence, the DR_{AMP} for the non-uniform nanogratings is lower than that for uniform nanogratings. But it is important to mention that the fabrication of uniform nano-gratings with completely parallel sidewalls is extremely difficult, while the proposed non-uniform nano-gratings (more specifically the GSNGs) can be easily fabricated with the presently existing nanofabrication and thin film deposition methods. Moreover, the DR_{AMP} values achieved for the proposed GNGs and GSNGs are sufficient to form a reliable SPR and SPRi sensing platforms.

When the results of the GNGs were compared with the GSNGs, it was observed that dips related to the plasmon resonance in the reflectance spectra are much deeper for the GNGs, and the values of differential reflectance amplitude (DR_{AMP}) are higher. The resonance dips are deeper in GNGs as light is more effectively coupled into the plasmonic waveguide modes in GNGs (whose unit cell resembles an MIM plasmonic waveguide structure. In contrast, the EM fields are confined not just in the central insulator layer in the case of GSNGs (whose unit cell resembles an IMIMI waveguide structure) but also in the outer HfO_2 insulator regions — as shown by the electric field maps shown in Fig. 6 and Fig. 7. This results in less enhancement of electromagnetic field in the narrow grooves of the GSNGs, which results in a smaller shift in the reflectance spectrum when the localized RI inside the narrow grooves is varied. Hence, the DR_{AMP} for the GSNGs is lower than that for GNGs.

We also studied the influence of changing the height of the GNGs, for a fixed nano-grating periodicity and groove width. With an increase in the height, 'H' of the GNGs, more number of dips related to the plasmon resonance appeared in the reflectance spectra (see Fig. 6). This can be attributed to light being coupled into a larger number of plasmonic waveguide modes in the deeper GNGs, i.e. the GNGs with a higher height 'H' can support a larger number of plasmonic waveguide modes.

The magnitudes of the differential reflectance amplitude (DR_{AMP}) for GNGs having groove width 'W' of 16.5 nm,

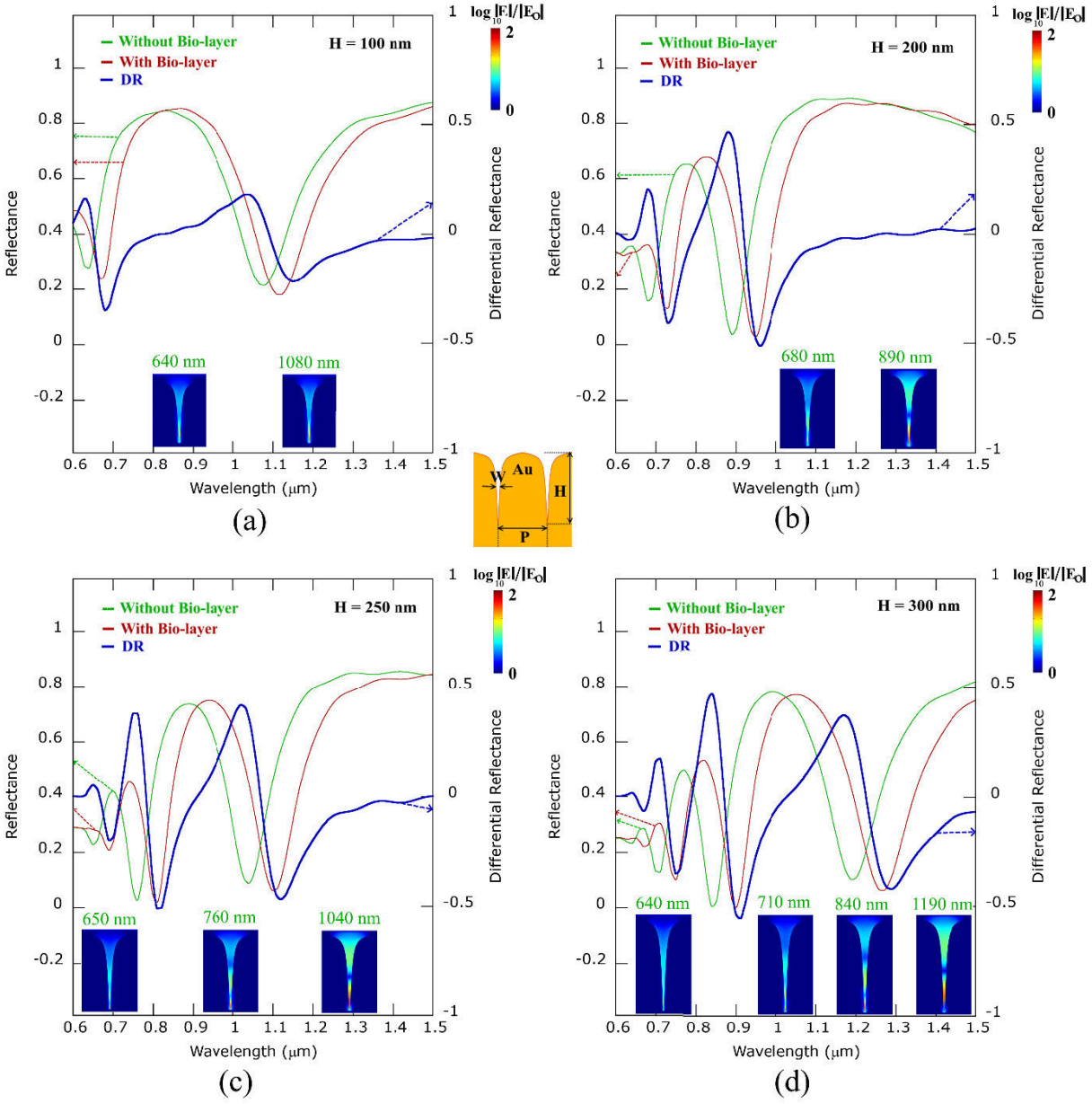

FIGURE 6. FDTD simulation results showing reflectance spectra and DR spectra for GNGs, for nano-grating heights 'H': (a) 100 nm (b) 200 nm (c) 250 nm and (d) 300 nm. The other nano-grating parameters are groove width 'W' = 16.5 nm and periodicity 'P' = 200 nm. The insets show electric field maps at different plasmon resonance dips in the reflectance spectra calculated for the case when no bio-layer is present on the nano-gratings.

periodicity 'P' of 200 nm, and heights 'H' of 100 nm, 200 nm, 250 nm and 300 nm were calculated to be 0.5125, 0.9794, 0.8920 and 1.027, respectively. It was observed that the magnitude of the DR_{AMP} is substantially higher for the GNGs with a height of 200 nm (or for heights greater than 200 nm) when compared with the DR_{AMP} of GNGs having a height of 100 nm. This can be attributed to deeper dips related to plasmon resonance in the reflectance spectra when the nanograting height is around 200 nm or higher (i.e. for the steep narrow groove nanogratings) as the incident optical radiation is more effectively coupled into the plasmonic waveguide modes in the GNGs. The higher value of DR_{AMP} can also be attributed to a larger red-shift in the reflectance spectrum (and in the plasmon resonance wavelength) for these steep narrow groove nano-gratings (H = 200 nm or higher) when the localized RI above the nano-grating surface was varied from 1.33 to 1.53. As the height of the groove is large (H = 200 nm or higher), light can be coupled into several plasmonic waveguide modes inside the narrow nanograting grooves of the GNGs which is also shown by the electric field maps in Fig. 6. Hence, more number of regions of high electromagnetic (EM) fields are present in

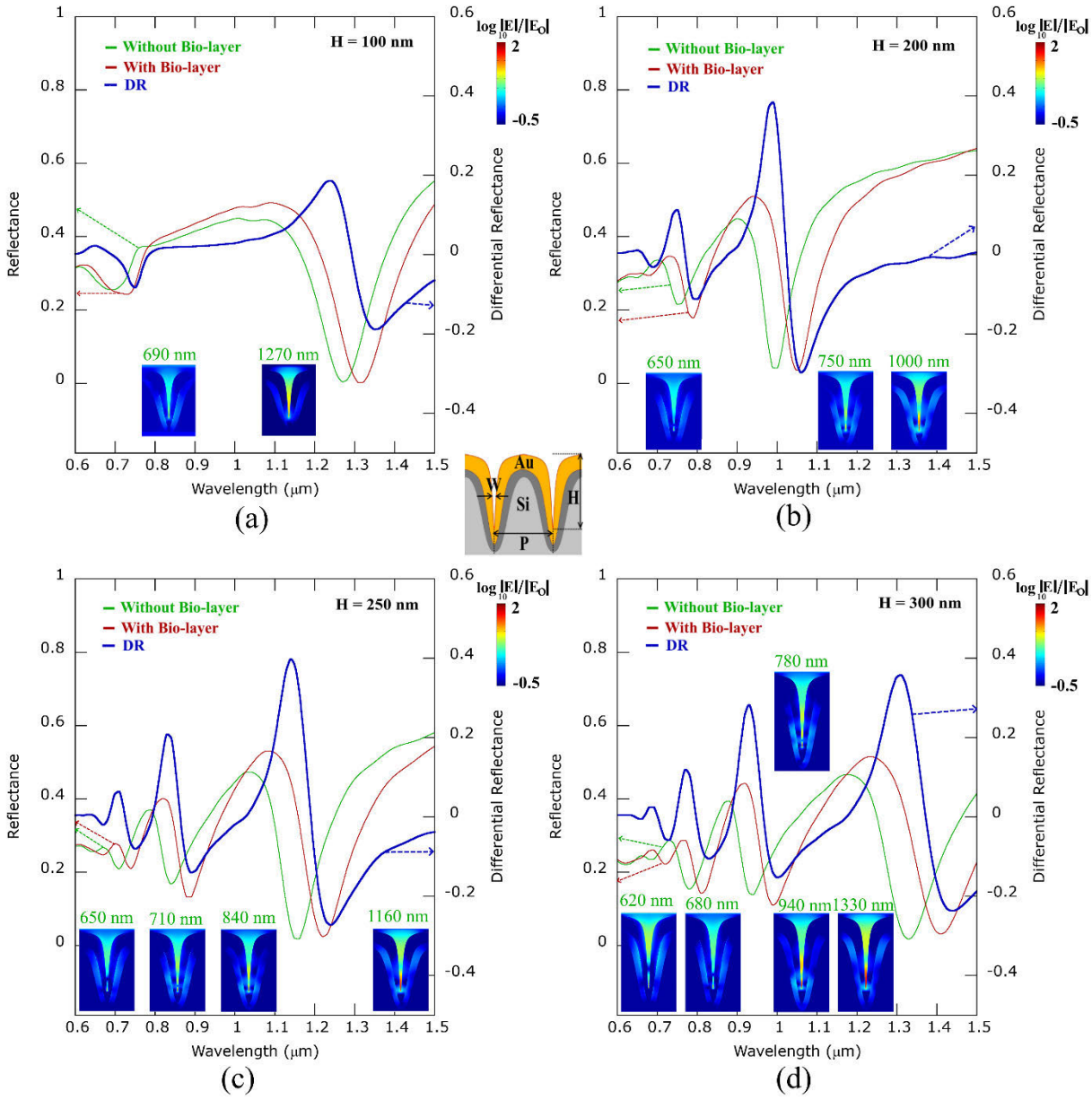

FIGURE 7. FDTD simulation results showing reflectance spectra and DR spectra for GSNGs, for nano-grating heights 'H': (a) 100 nm (b) 200 nm (c) 250 nm and (d) 300 nm. The other nano-grating parameters are groove width 'W' = 16.5 nm and periodicity 'P' = 200 nm. The insets show electric field maps at different plasmon resonance dips in the reflectance spectra calculated for the case when no bio-layer is present on the nano-gratings.

each groove, resulting in a larger red-shift in the reflectance spectrum for the nanogratings.

A similar trend of the variation of the DR spectra with the nano-grating height was observed in the case of GSNGs (see Fig. 7). Similar to the case of GNGs, a greater number of dips related to the plasmon resonance appeared in the reflectance spectra as the height of the GSNGs was increased (See Fig. 7). This can be attributed to light being coupled into a larger number of plasmonic waveguide modes in the deeper nanogratings. The electric field maps of the different plasmonic waveguide modes are also shown in Figs. 7 (a)-(d). Moreover, it was observed that the DR spectra of the GSNGs are red-shifted as compared to the DR spectra of the GNGs (See Fig. 6 and 7). Light is effectively coupled into plasmonic waveguide modes for GNGs (whose unit cell resembles an MIM plasmonic waveguide structure. In contrast, the optical EM fields are not entirely confined inside the narrow grooves of the GSNGs (whose unit cell resembles an IMIMI plasmonic waveguide structure). This is because the electromagnetic fields also exist in the outer insulator regions (HFO_2) of the IMIMI waveguide-like structure, which has a higher refractive index as compared to the central insulator region

TABLE 1. DR_{AMP} values for GNGs with 'W' = 8.25 nm.

H (nm)	P = 100 nm	P = 150 nm	P = 200 nm	P = 250 nm
100	1.0602	1.1390	1.0435	1.0246
150	1.1853	1.3862	1.4309	1.4256
200	1.0602	1.2867	1.3813	1.4034
250	1.1342	1.2673	1.2867	1.2882

TABLE 2. DR_{AMP} values for GSNGs with 'W' = 8.25 nm.

H (nm)	P = 100 nm	P = 150 nm	P = 200 nm	P = 250 nm
100	0.3165	0.4174	0.5727	0.6989
150	0.3380	0.6486	0.8728	0.9832
200	0.3629	0.6408	0.8571	1.0363
250	0.3757	0.6407	0.8822	1.0076

TABLE 3. DR_{AMP} values for GNGs and GSNGs with 'P' = 200 nm and 'H' = 200 nm.

W (nm)	GNG	GSNG
8.25	1.3813	0.8571
12.375	1.2437	0.8297
16.5	0.9794	0.6815
24.75	0.5562	0.3506

(water or aqueous buffer solution). This is also shown in the electric field maps in Figs. 7 (a)-(d). This explains the red-shift of the reflectance spectra in the case of the GSNGs as compared to the GNGs.

The magnitudes of the differential reflectance amplitude (DR_{AMP}) for the GSNGs were calculated to be 0.3748, 0.6815, 0.6696 and 0.5945 for the nano-grating periodicity of 200 nm, groove width of 16.5 nm, and heights of 100 nm, 200 nm, 250 nm and 300 nm, respectively. It can be observed from Fig. 6 and 7 that the values of DR_{AMP} for the GSNGs are lower than those for the GNGs. This can be attributed to a lower shift in the reflectance spectrum when the localized RI inside the narrow grooves of the GSNGs is varied (explained earlier). Moreover, it can be attributed to less deep dips related to the plasmon resonance in the reflectance spectra for the GSNGs when compared with those for GNGs (explained earlier).

The effect of varying the groove widths 'W' of proposed GNGs and GSNGs on the DR spectra was also studied. The results of the FDTD calculations displaying the influence of varying the groove width 'W' of the nano-gratings are shown in Figs. 8 and 9 for the GNGs and the GSNGs, respectively. It was observed that there was a reduction in the number of plasmonic waveguide modes as the groove width 'W' was increased. When the groove width increases, light is not effectively coupled into plasmonic waveguide modes of the nanograting, and as a result, there is a reduction in the number of plasmonic waveguide modes.

The effects of variation in the height, periodicity, and groove width of the GNGs and the GSNGs on DR_{AMP} values are presented in Tables 1 to 3. One can observe from Table 3 that there is a significant decrease in the value of the DR_{AMP} as the groove width 'W' of the GNGs is increased. When the groove width increases, light is not effectively coupled into plasmonic waveguide modes of the GNGs (whose unit cell resembles an MIM plasmonic waveguide structure. This results in less enhancement of electromagnetic fields (as also shown by the electric field maps shown in Fig. 8) in the grooves of the nanograting, which in turn results in a lower spectral shift when the localized refractive index inside the narrow grooves is varied. As a result, there is a decrease in the value of the DR_{AMP}. Similarly, one can observe from Table 3 that there is a significant decrease in the value of the DR_{AMP} as the groove width 'W' of the GSNGs is increased. In case of GSNGs also, as the groove width 'W' is increased, there is reduced enhancement of electromagnetic fields (as also shown by the electric field maps shown in Fig. 8) in nanograting grooves resulting in a lower shift in the reflectance spectrum when the localized refractive index inside the narrow nanograting grooves is varied.

The values of the nano-grating periodicity 'P', height 'H', and groove width 'W' were optimized so as to get the maximum values of DR_{AMP} and the optimal values are provided in Tables 1 to 3. It has to be noted that a significantly large magnitude of differential reflectance amplitude ($DR_{AMP} > 1.2$) is obtainable for uniform rectangular aperture gold nano-gratings. However, the fabrication of uniform nano-gratings with completely parallel sidewalls is not feasible. For the GNGs, the highest value of the DR_{AMP} of 1.4309 was calculated for the nano-gratings periodicity 'P' = 200 nm, height 'H' = 150 nm, and groove width 'W' = 8.25 nm. This value of differential reflectance amplitude ($DR_{AMP} = 1.4309$) is significantly higher when compared to the value calculated for a 40 nm thick plain gold film in the Kretschmann configuration ($DR_{AMP} = 0.2766$). However, it must be pointed out that the GNGs are also not very easy to fabricate. On the other hand, the GSNGs being proposed can be easily fabricated with the presently existing nanofabrication and thin film deposition methods. For the GSNGs, the highest value of the differential reflectance amplitude of 1.0363 was calculated for the nano-gratings periodicity 'P' = 250 nm, height 'H' = 200 nm, and groove width 'W' = 8.25 nm. This value of differential reflectance amplitude ($DR_{AMP} = 1.0363$) is also significantly higher compared to the value calculated for a 40 nm thick plain gold film in the Kretschmann configuration ($DR_{AMP} = 0.2766$).

The biosensing or surface sensing is defined as the ratio of the shift in the plasmon resonance wavelength due to per unit length of the biomolecules [51], [52].

$$S_S = \frac{\Delta\lambda_S}{\Delta l} nm/nm \tag{1}$$

The figure of merit of the localized sensor is defined as the ratio of localized sensitivity and full width half maximum

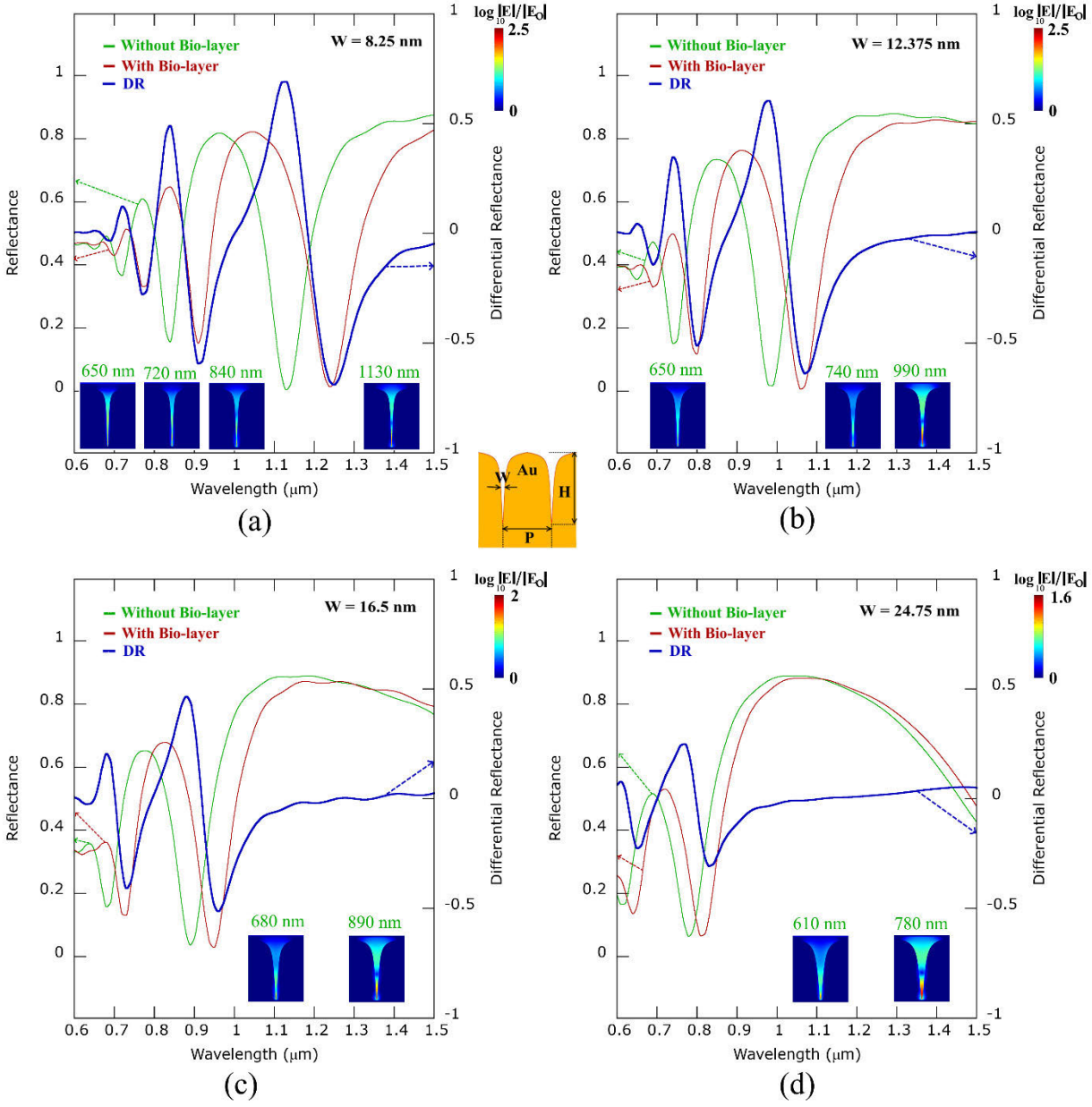

FIGURE 8. FDTD simulation results showing reflectance spectra and DR spectra for GNGs, for nano-grating groove widths 'W': (a) 8.25 nm, (b) 12.375 nm, (c) 16.5 nm, and (d) 24.75 nm. The other nano-grating parameters are height 'H' = 200 nm and periodicity 'P' = 200 nm. The insets show electric field maps at different plasmon resonance dips in the reflectance spectra calculated for the case when no bio-layer is present on the nano-gratings.

(FWHM) of the corresponding plasmonic dip [51], [52].

$$FOM_S = \frac{S_S}{\text{FWHM}} nm^{-1} \tag{2}$$

The values of surface sensitivity (S_S) for different structural parameters of the narrow groove nano-grating sensors are given in Tables 4 to 6. We observe a maximum S_S of $\approx$ 70 nm/nm which is much larger than that obtained for the thin film SPR sensors (which provide a maximum S_S of $\approx$ 14 nm/nm). We can observe from Tables 4 and 5 that for certain values of height and periodicity of the nanogratings, there are multiple plasmon resonance dips in the reflectance spectra and that these dips shift by different values upon changing the refractive index (from 1.33 to 1.53) of the media around

TABLE 4. S_S (IN nm/nm) for GNGs with 'W' = 8.25 nm.

H (nm)	P = 100 nm	P = 150 nm	P = 200 nm	P = 250 nm
100	30	35	30, 55	35, 55
150	40	30, 40	30, 45	25, 45
200	40, 55	40, 55	35, 55	35, 55
250	45, 70	45, 65	45, 70	40, 60

TABLE 5. S_S (IN nm/nm) for GSNGs with 'W' = 8.25 nm.

H (nm)	P = 100 nm	P = 150 nm	P = 200 nm	P = 250 nm
100	35	30	35	30
150	30, 50	25, 45	30, 45	30, 40
200	30, 40	35, 65	35, 60	35, 55
250	30, 45	30, 40	30, 45	35, 40

TABLE 6. S_S (IN nm/nm) for GNGs and GSNGs with 'P' = 200 nm and 'H' = 200 nm.

W (nm)	GNG	GSNG
8.25	55	60
12.375	35	40
16.5	30	30
24.75	15	15

TABLE 7. FOM_S (IN nm^{-1}) for GNGs with 'W' = 8.25 nm.

H (nm)	P = 100 nm	P = 150 nm	P = 200 nm	P = 250 nm
100	0.55	0.64	1.30, 1.06	0.74, 0.28
150	0.47	0.75, 0.50	0.75, 0.64	0.66, 0.69
200	0.72, 0.61	0.80, 0.49	0.78, 0.61	0.74, 0.58
250	0.64, 0.39	0.69, 0.39	0.92, 0.47	0.70, 0.45

TABLE 8. FOM_S (IN nm^{-1}) for GSNGs with 'W' = 8.25 nm.

H (nm)	P = 100 nm	P = 150 nm	P = 200 nm	P = 250 nm
100	0.44	0.60	0.29	0.25
150	0.23	0.50, 0.38	1.50, 0.90	0.80
200	0.43, 0.44	0.50, 0.36	1.40, 0.79	0.88, 0.92
250	0.30, 0.19	0.50, 0.26	0.38, 0.41	0.70, 0.50

the surface of these nano-gratings. The resonance dips have different shifts as the refractive index is varied as the surface sensitivity (S_S) is always higher for longer wavelengths. This was shown in [27] for both prism coupling and grating coupling. Moreover, the fact that sensitivity is always higher for longer wavelengths is also shown by us mathematically in the Appendix.

We can observe from Table 6 that as the groove width 'W' is decreased, the maximum surface sensitivity (S_S), increases for both the GNGs and the GSNGs. As the groove width decreases, incident optical radiation is effectively coupled into plasmonic waveguide modes of the GNGs (whose unit cell resembles an MIM plasmonic waveguide structure. This results in more EM field enhancement in nanograting grooves, which in turn results in a higher shift in the reflectance spectrum when the localized refractive index inside the narrow grooves is varied. The same reasoning can explain the increase of S_S in gold-coated silicon nanogratings with a decrease in the groove width 'W' (as can be seen from Table 6).

The values of FOM_S are also calculated for narrow groove nanogratings. FOM_S values of proposed structures are shown

TABLE 9. FOM_S (IN nm^{-1}) for GNGs and GSNGs with 'P' = 200 nm and 'H' = 200 nm.

W (nm)	GNG	GSNG
8.25	0.78, 0.61	1.40, 0.79
12.375	0.33	0.40
16.5	0.38	0.38
24.75	0.40	0.33

TABLE 10. Surface and bulk sensitivities of different plasmonic sensors.

Structure	S_B (nm/RIU)	FOM_B (RIU^{-1})	S_S (nm/nm)	FOM_S (nm^{-1})	References
Nanosphere	76	0.6	-	-	[57-59]
Nanorods	195-288	2.6	-	-	[59,60]
Nanopyramid	540	4.5	-	-	[59]
Metamaterial	558	3.8	-	-	[61]
Nanostar	879	10.7	-	-	[62]
Nanoellipsoid	-	~5	~8	0.20	[51]
Nanorings	1300	5	12	0.035	[52]
Grating	120	8	~2.1*	~0.14*	[53]
Nanohole array	436	4.91	~1.38*	~0.016*	[54]
Nanohole array	183	1.7	~2.5*	~0.33*	[55]
Fiber nanoprobe	432	~2.9	~0.41*	~0.0028*	[56]
PCF	50000	355	-	-	[61]
Exposed-core PCF	34000	310	-	-	[62]
PCF	111000	2050	-	-	[63]
PCF	62000	1415	-	-	[64]
Grating	1100	20	-	-	[65]
This work	1010	16	70	1.5	

*Calculated using (1) and (2)

in Tables 7−9. FOM_S are higher for the plasmon resonances at lower wavelengths as at lower wavelengths the FWHM values are smaller. We also observe that for higher FOM_S, the intensity variation in the value of reflectance (for a given plasmon mode) is very small. Hence, it is difficult to detect the change in the signal for intensity based detection. In this case, the DR_{AMP} values are more effective for characterizing the performance of the proposed sensor.

The surface sensitivity (S_S) of the nanogratings proposed in this article is significantly higher than what has been reported in previous literature [51]–[56]. Table 10 shows that the value of surface sensitivity of the proposed nanogratings is 70 nm/nm while that reported in previous literature is less than 13 nm/nm. Moreover, the figure of merit of the localized sensor (FOM_S) for our proposed nanograting sensors is 1.5 nm^{-1}, which is significantly higher than what has been reported previously (< 0.5 nm^{-1}).

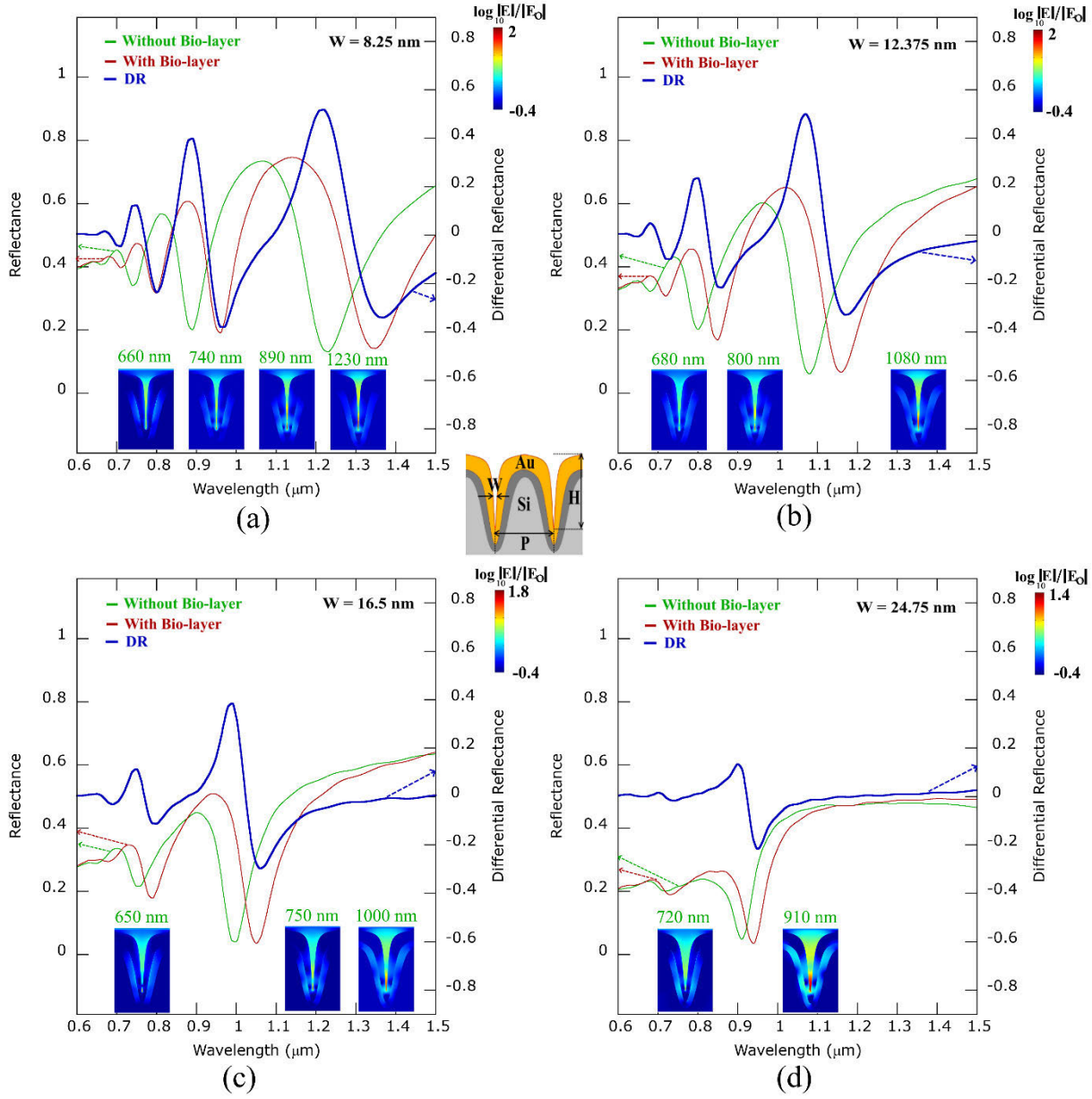

FIGURE 9. FDTD simulation results showing reflectance spectra and DR spectra for GSNGs, for nano-grating groove widths 'W': (a) 8.25 nm, (b) 12.375 nm, (c) 16.5 nm, and (d) 24.75 nm. The other nano-grating parameters are height 'H' = 200 nm and periodicity 'P' = 200 nm. The insets show electric field maps at different plasmon resonance dips in the reflectance spectra calculated for the case when no bio-layer is present on the nano-gratings.

Although the sensors proposed in the paper are localized sensors with high values of surface sensitivity (S_S), we have also calculated the bulk sensitivity of the proposed nanograting structures. The bulk sensitivity of the plasmonic sensors is calculated by taking the ratio of the shift in the plasmon resonance wavelength ($\Delta\lambda$) and the change in the bulk refractive index (Δn) that causes the shift in the resonance wavelength [3], [9], [28], [51]–[67].

$$S_B = \frac{\Delta\lambda_B}{\Delta n_B} nm/RIU \tag{3}$$

The figure of merit (FOM_{bulk}) [51]–[67] associated with bulk sensing is defined as follows:

$$FOM_B = \frac{S_B}{\text{FWHM}} RIU^{-1} \tag{4}$$

where FWHM is the full width half maximum of the plasmon resonance dips.

The bulk sensitivity is usually less for the localized sensors as the electric field decay length (i.e. the penetration depth) is very small for localized sensors [2], [28]. Table 10 shows a comparison of the bulk sensitivity of the proposed nanogratings with those of previously reported plasmonic sensors. The

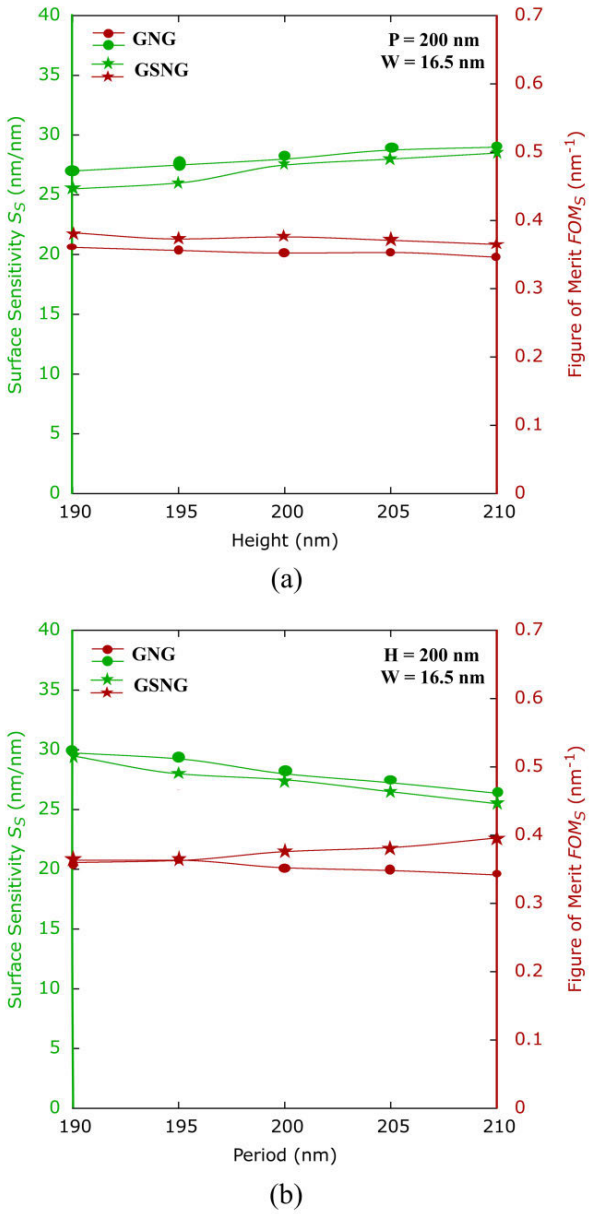

FIGURE 10. FDTD simulation results showing the effect of change in: (a) Height, and (b) Periodicity on the biosensing performance of the GNGs and GSNGs.

proposed nanograting structure shows a better bulk sensing performance compared to LSPR sensors [51]–[62]. Although the photonic crystal fiber (PCF) based SPR sensors [63]–[66] show very high bulk sensitivity but calculations of surface sensitivity have not been provided in those papers. Hence, we cannot compare the surface sensitivity performance of our proposed sensors with the PCF based sensors.

We can also observe from Figs. 9 (a)-(c) that there are multiple plasmon resonance related dips present in the reflectance spectra of the proposed nanogratings and that the resonance wavelength of these dips can be tuned by varying the structural parameters of the nanogratings. The multiple spectral bands allow sensing at different plasmon resonance wavelengths for intensity based plasmonic sensing — this can allow tuning the structural parameters to achieve the plasmonic dips at some desired wavelengths of interest for which light sources (laser diodes or LEDs) are available, thereby enabling intensity based sensing at these wavelengths.

We observe from Fig. 10 that varying the structural parameters of the proposed nanogratings such as the height and periodicity do not lead to significant changes in the biosensing performance characteristics such as surface sensitivity (S_S) figure of merit of the localized sensor (FOM_S). This shows the robustness of the proposed nanogratings to variations (in the dimensions of the nanograting structural parameters) which could be caused by variability in the fabrication process.

In this article, we have shown that the proposed non-uniform nano-gratings can easily couple the normally incident optical radiation into surface plasmons, and significantly high magnitudes of DR_{AMP} were achieved. These large values of DR_{AMP} indicate a very high sensitivity of the SPR and SPRi sensors employing these nano-gratings to localized RI changes around the nanogratings. Furthermore, the plasmon resonance dips can be obtained in the desired spectral regimes by engineering the different geometrical parameters of these nano-gratings. This provides the freedom to select the desired wavelengths for the designed SPR and SPRi sensors based on the nanograting, thereby providing a reliable platform for SPR or SPRi based sensing. The non-uniform gold-coated silicon nanogratings being proposed can be easily fabricated with the presently existing nanofabrication and thin film deposition methods.

IV. CONCLUSION

In this article, we have presented 'practically realizable' SPR sensing and imaging sensors utilizing the non-uniform narrow-groove gold nanogratings. We have presented the optical characteristics of two kinds of narrow-groove plasmonic nanogratings: gold nanogratings and gold-coated silicon nanograting, and have compared their results with those of uniform rectangular aperture nano-gratings and the conventional surface plasmon resonance sensors based on a continuous gold film and prism coupling (Kretschmann configuration). By employing finite difference time domain calculations, we have demonstrated that very high magnitudes of DR_{AMP} (which is indicative of high sensitivity of the SPR or SPRi sensors for changes in localized refractive index) are obtained for these nano-gratings and that these values of DR_{AMP} are significantly higher compared to values calculated for a plain gold film in the Kretschmann configuration. The sensors being proposed in this article provide a maximum sensitivity of localized refractive index sensing (i.e. surface sensitivity or S_S) of 70 nm/nm with a figure of merit of the localized sensor (FOM_S) of 1.5 nm^{-1}. This sensitivity of localized refractive index sensing is the highest reported thus far in comparison with previously reported plasmonic sensors. The proposed non-uniform nanogratings

do not require any complex surface plasmon coupling mechanism, as is required in the conventional SPR sensors based on a continuous gold film (i.e. the Kretschmann configuration). In the non-uniform plasmonic nano-gratings being proposed, we have shown that normally incident light can be coupled directly into surface plasmons. Moreover, we have demonstrated that the wavelengths — at which the plasmon resonance-related dips in the reflectance spectra occur — can be tuned by varying the geometrical parameters of these non-uniform nano-gratings (such as the nano-grating periodicity, groove width, and height). Finally, non-uniform gold-coated silicon nano-gratings can be easily fabricated with the presently existing nanofabrication and thin film deposition methods.

APPENDIX

The effective refractive index of the coupled surface plasmon is expressed as

$$n_{eff} = \frac{\sqrt{\varepsilon_{mr} n_d^2}}{\sqrt{\varepsilon_{mr} + n_d^2}} \tag{5}$$

where, ε_{mr} is the metal-dielectric function at coupled plasmon resonance wavelength λ and n_d is the refractive index of the dielectric on top of the metal surface. Differentiating both sides of (5) w.r.t. n_d

$$\frac{\partial n_{eff}}{\partial n_d} = \frac{n_d^2 \frac{d\varepsilon_{mr}}{d\lambda}\frac{d\lambda}{dn_d} + 2\varepsilon_{mr} n_d}{2\sqrt{\varepsilon_{mr} n_d^2}} \sqrt{\varepsilon_{mr} + n_d^2} - \frac{\sqrt{\varepsilon_{mr} n_d^2}\left(\frac{d\varepsilon_{mr}}{d\lambda}\frac{d\lambda}{dn_d} + 2n_d\right)}{2\left(\varepsilon_{mr} + n_d^2\right)^{\frac{3}{2}}} \tag{6}$$

Solving (2) for $\frac{d\lambda}{dn_d}$ (shift in resonance wavelength with a small change in the dielectric refractive index)

$$\frac{d\lambda}{dn_d} = \frac{2\sqrt{\varepsilon}_{mr}\left(\varepsilon_{mr} + n_d^2\right)^{\frac{3}{2}}\frac{\partial n_{eff}}{\partial n_d} - 2\varepsilon_{mr}^2}{n_d^3 \frac{d\varepsilon_{mr}}{d\lambda}} \tag{7}$$

The first term in the numerator is very small compared to ε_{mr}^2 as change in n_{eff} is very small with the change in n_d. So,

$$\frac{d\lambda}{dn_d} = \frac{-2\varepsilon_{mr}^2}{n_d^3 \frac{d\varepsilon_{mr}}{d\lambda}} \tag{8}$$

For the purpose of this proof, a simplified model such as the Drude model for metals can be taken to express the metal-dielectric function using the following equation:

$$\varepsilon_{mr} = 1 - \frac{\omega_p^2}{\omega^2} \tag{9}$$

where, ω_p is the plasma frequency of free electrons and $\omega = 2\pi c/\lambda$. c is the speed of light in vacuum. So,

$$\varepsilon_{mr} = 1 - \frac{\omega_p^2}{\left(2\pi c/\lambda\right)^2}$$

$$\varepsilon_{mr} = 1 - a\lambda^2 \tag{10}$$

where, $a = \frac{\omega_p^2}{(2\pi c)^2}$

So we can have

$$\frac{d\lambda}{dn_d} = \frac{\left(a\lambda^2 - 1\right)^2}{a\lambda n_d^3} \tag{11}$$

The value of plasma frequency $\omega_p = 1.323X10^{16} s^{-1}$ for gold is calculated in [68]. The corresponding value of $a = 49.26\ \mu m^{-2}$. So for $\lambda = 785$ nm, the value of $\varepsilon_{mr} \sim -29.36$ calculated using (10). Moreover, the magnitude of ε_{mr} increases for the longer wavelengths ($\varepsilon_{mr} \propto \lambda^2$). Hence, the shift in resonance wavelength ($d\lambda$) on changing the refractive index (n_d) of the dielectric layer is higher for longer wavelengths as compared to shorter wavelengths.

REFERENCES

[1] H. Raether, *Surface Plasmons on Smooth and Rough Surfaces and on Gratings*. Berlin, Germany: Springer-Verlag, 1988.
[2] S. A. Maier, *Plasmonics: Fundamentals and Applications*. New York, NY, USA: Springer, 2007.
[3] J. Homola, S. S. Yee, and G. Gauglitz, "Surface plasmon resonance sensors: Review," *Sens. Actuators B, Chem.*, vol. 54, nos. 1–2, pp. 3–15, Jan. 1999.
[4] J. Homola, "On the sensitivity of surface plasmon resonance sensors with spectral interrogation," *Sens. Actuators B, Chem.*, vol. 41, nos. 1–3, pp. 207–211, Jun. 1997.
[5] R. C. Jorgenson and S. S. Yee, "A fiber-optic chemical sensor based on surface plasmon resonance," *Sens. Actuators B, Chem.*, vol. 12, no. 3, pp. 213–220, Apr. 1993.
[6] R. Slavík, J. Homola, and J. Čtyroký, "Single-mode optical fiber surface plasmon resonance sensor," *Sens. Actuators B, Chem.*, vol. 54, nos. 1–2, pp. 74–79, Jan. 1999.
[7] R. Slavík, J. Homola, J. Čtyroký, and E. Brynda, "Novel spectral fiber optic sensor based on surface plasmon resonance," *Sens. Actuators B, Chem.*, vol. 74, nos. 1–3, pp. 106–111, Apr. 2001.
[8] A. J. Haes and R. P. Van Duyne, "A unified view of propagating and localized surface plasmon resonance biosensors," *Anal. Bioanal. Chem.*, vol. 379, nos. 7–8, pp. 920–930, Aug. 2004.
[9] A. D. McFarland and R. P. Van Duyne, "Single silver nanoparticles as real-time optical sensors with zeptomole sensitivity," *Nano Lett.*, vol. 3, no. 8, pp. 1057–1062, Aug. 2003.
[10] G. Mie, "Beiträge zur optik trüber medien, speziell kolloidaler metallösungen," *Annalen der Physik*, vol. 330, no. 3, pp. 377–445, 1908.
[11] J. J. Mock, D. R. Smith, and S. Schultz, "Local refractive index dependence of plasmon resonance spectra from individual nanoparticles," *Nano Lett.*, vol. 3, no. 4, pp. 485–491, Apr. 2003.
[12] C. F. Bohren and D. R. Huffman, "Absorption and scattering by a sphere," in *Absorption and Scattering of Light by Small Particles*. Weinheim, Germany: Wiley-VCH, 1998, pp. 82–129.
[13] H. C. van de Hulst, *Light Scattering by Small Particles*, 1st ed. New York, NY, USA: Dover, 1981.
[14] B.-B. Xu, Z.-C. Ma, H. Wang, X.-Q. Liu, Y.-L. Zhang, X.-L. Zhang, R. Zhang, H.-B. Jiang, and H.-B. Sun, "A SERS-active microfluidic device with tunable surface plasmon resonances," *Electrophoresis*, vol. 32, no. 23, pp. 3378–3384, Dec. 2011.
[15] D.-H. Kuan, I.-S. Wang, J.-R. Lin, C.-H. Yang, C.-H. Huang, Y.-H. Lin, C.-T. Lin, and N.-T. Huang, "A microfluidic device integrating dual CMOS polysilicon nanowire sensors for on-chip whole blood processing and simultaneous detection of multiple analytes," *Lab Chip*, vol. 16, no. 16, pp. 3105–3113, 2016.
[16] J. Gamby, A. Rudolf, M. Abid, H. H. Girault, C. Deslouis, and B. Tribollet, "Polycarbonate microchannel network with carpet of gold nanowires as SERS-active device," *Lab Chip*, vol. 9, no. 12, pp. 1806–1808, Jun. 2009.
[17] I.-F. Cheng, C.-C. Lin, D.-Y. Lin, and H.-C. Chang, "A dielectrophoretic chip with a roughened metal surface for on-chip surface-enhanced Raman scattering analysis of bacteria," *Biomicrofluidics*, vol. 4, no. 3, Sep. 2010, Art. no. 034104.

[18] R. A. Pala, J. White, E. Barnard, J. Liu, and M. L. Brongersma, "Design of plasmonic thin-film solar cells with broadband absorption enhancements," *Adv. Mater.*, vol. 21, no. 34, pp. 3504–3509, Sep. 2009.

[19] Y. Sharma, V. A. Tiruveedhula, J. F. Muth, and A. Dhawan, "VO_2 based waveguide-mode plasmonic nano-gratings for optical switching," *Opt. Exp.*, vol. 23, no. 5, p. 5822, 2015.

[20] R. Alvarez-Puebla, B. Cui, J.-P. Bravo-Vasquez, T. Veres, and H. Fenniri, "Nanoimprinted SERS-active substrates with tunable surface plasmon resonances," *J. Phys. Chem. C*, vol. 111, no. 18, pp. 6720–6723, May 2007.

[21] M. Fleischmann, P. J. Hendra, and A. J. McQuillan, "Raman spectra of pyridine adsorbed at a silver electrode," *Chem. Phys. Lett.*, vol. 26, no. 2, pp. 163–166, May 1974.

[22] S. Schlücker, Ed., *Surface Enhanced Raman Spectroscopy: Analytical, Biophysical and Life Science Applications*. Weinheim, Germany: Wiley-VCH, 2011.

[23] T. Vo-Dinh, "Surface-enhanced Raman spectroscopy using metallic nanostructures," *TrAC Trends Anal. Chem.*, vol. 17, nos. 8–9, pp. 557–582, 1998.

[24] D. L. Jeanmaire and R. P. Van Duyne, "Surface Raman spectroelectrochemistry: Part I. Heterocyclic, aromatic, and aliphatic amines adsorbed on the anodized silver electrode," *J. Electroanal. Chem.*, vol. 84, no. 1, pp. 1–20, 1977.

[25] M. Bauch, K. Toma, M. Toma, Q. Zhang, and J. Dostalek, "Plasmon-enhanced fluorescence biosensors: A review," *Plasmonics*, vol. 9, no. 4, pp. 781–799, Aug. 2014.

[26] P. Genevet, J.-P. Tetienne, E. Gatzogiannis, R. Blanchard, M. A. Kats, M. O. Scully, and F. Capasso, "Large enhancement of nonlinear optical phenomena by plasmonic nanocavity gratings," *Nano Lett.*, vol. 10, no. 12, pp. 4880–4883, Dec. 2010.

[27] J. Homola, I. Koudela, and S. S. Yee, "Surface plasmon resonance sensors based on diffraction gratings and prism couplers: Sensitivity comparison," *Sens. Actuators B, Chem.*, vol. 54, nos. 1–2, pp. 16–24, Jan. 1999.

[28] S. Roh, T. Chung, and B. Lee, "Overview of the characteristics of micro- and nano-structured surface plasmon resonance sensors," *Sensors*, vol. 11, no. 2, pp. 1565–1588, Jan. 2011.

[29] J. B. Beusink, A. M. C. Lokate, G. A. J. Besselink, G. J. M. Pruijn, and R. B. M. Schasfoort, "Angle-scanning SPR imaging for detection of biomolecular interactions on microarrays," *Biosensors Bioelectron.*, vol. 23, no. 6, pp. 839–844, Jan. 2008.

[30] S. Scarano, M. Mascini, A. P. F. Turner, and M. Minunni, "Surface plasmon resonance imaging for affinity-based biosensors," *Biosensors Bioelectron.*, vol. 25, no. 5, pp. 957–966, Jan. 2010.

[31] C. L. Wong and M. Olivo, "Surface plasmon resonance imaging sensors: A review," *Plasmonics*, vol. 9, no. 4, pp. 809–824, Aug. 2014.

[32] R. D'Agata and G. Spoto, "Surface plasmon resonance imaging for nucleic acid detection," *Anal. Bioanal. Chem.*, vol. 405, nos. 2–3, pp. 573–584, Jan. 2013.

[33] K. Ma, D. J. Kim, K. Kim, S. Moon, and D. Kim, "Target-localized nanograting-based surface plasmon resonance detection toward label-free molecular biosensing," *IEEE J. Sel. Topics Quantum Electron.*, vol. 16, no. 4, pp. 1004–1014, Jul. 2010.

[34] K. Kim, D. J. Kim, E.-J. Cho, J.-S. Suh, Y.-M. Huh, and D. Kim, "Nanograting-based plasmon enhancement for total internal reflection fluorescence microscopy of live cells," *Nanotechnology*, vol. 20, no. 1, Jan. 2009, Art. no. 015202.

[35] A. A. Grunin, A. G. Zhdanov, A. A. Ezhov, E. A. Ganshina, and A. A. Fedyanin, "Surface-plasmon-induced enhancement of magneto-optical kerr effect in all-nickel subwavelength nanogratings," *Appl. Phys. Lett.*, vol. 97, no. 26, Dec. 2010, Art. no. 261908.

[36] A. Normatov, P. Ginzburg, N. Berkovitch, G. M. Lerman, A. Yanai, U. Levy, and M. Orenstein, "Efficient coupling and field enhancement for the nano-scale: Plasmonic needle," *Opt. Exp.*, vol. 18, no. 13, pp. 14079–14086, 2010.

[37] M. B. Sobnack, W. C. Tan, N. P. Wanstall, T. W. Preist, and J. R. Sambles, "Stationary surface plasmons on a zero-order metal grating," *Phys. Rev. Lett.*, vol. 80, no. 25, pp. 5667–5670, Jun. 1998.

[38] A. Dhawan, M. Canva, and T. Vo-Dinh, "Narrow groove plasmonic nano-gratings for surface plasmon resonance sensing," *Opt. Exp.*, vol. 19, no. 2, pp. 787–813, 2011.

[39] W.-C. Tan, T. W. Preist, J. R. Sambles, and N. P. Wanstall, "Flat surface-plasmon-polariton bands and resonant optical absorption on short-pitch metal gratings," *Phys. Rev. B, Condens. Matter*, vol. 59, no. 19, pp. 12661–12666, May 1999.

[40] I. R. Hooper and J. R. Sambles, "Surface plasmon polaritons on thin-slab metal gratings," *Phys. Rev. B, Condens. Matter*, vol. 67, no. 23, Jun. 2003, Art. no. 235404.

[41] T. López-Rios, D. Mendoza, F. J. García-Vidal, J. Sánchez-Dehesa, and B. Pannetier, "Surface shape resonances in lamellar metallic gratings," *Phys. Rev. Lett.*, vol. 81, no. 3, pp. 665–668, Jul. 1998.

[42] F. J. Garcia-Vidal, J. Sanchez-Dehesa, A. Dechelette, E. Bustarret, T. Lopez-Rios, T. Fournier, and B. Pannetier, "Localized surface plasmons in lamellar metallic gratings," *J. Lightw. Technol.*, vol. 17, no. 11, pp. 2191–2195, 1999.

[43] J. A. Porto, F. J. García-Vidal, and J. B. Pendry, "Transmission resonances on metallic gratings with very narrow slits," *Phys. Rev. Lett.*, vol. 83, no. 14, pp. 2845–2848, Oct. 1999.

[44] F. J. García-Vidal and L. Martín-Moreno, "Transmission and focusing of light in one-dimensional periodically nanostructured metals," *Phys. Rev. B, Condens. Matter*, vol. 66, no. 15, Oct. 2002, Art. no. 155412.

[45] H.-N. Wang, A. Dhawan, Y. Du, D. Batchelor, D. N. Leonard, V. Misra, and T. Vo-Dinh, "Molecular sentinel-on-chip for SERS-based biosensing," *Phys. Chem. Chem. Phys.*, vol. 15, no. 16, p. 6008, 2013.

[46] A. Taflove and S. C. Hagness, *Computational Electrodynamics: The Finite-Difference Time-Domain Method*, 2nd ed. Norwood, MA, USA: Artech House, 2000.

[47] P. B. Savaliya, A. Thomas, R. Dua, and A. Dhawan, "Tunable optical switching in the near-infrared spectral regime by employing plasmonic nanoantennas containing phase change materials," *Opt. Exp.*, vol. 25, no. 20, pp. 23755–23772, 2017.

[48] M. G. Moharam and T. K. Gaylord, "Rigorous coupled-wave analysis of planar-grating diffraction," *J. Opt. Soc. Amer.*, vol. 71, no. 7, pp. 811–818, Jul. 1981.

[49] M. G. Moharam, E. B. Grann, D. A. Pommet, and T. K. Gaylord, "Formulation for stable and efficient implementation of the rigorous coupled-wave analysis of binary gratings," *J. Opt. Soc. Amer. A, Opt. Image Sci.*, vol. 12, no. 5, pp. 1068–1076, 1995.

[50] P. Arora, E. Talker, N. Mazurski, and U. Levy, "Dispersion engineering with plasmonic nano structures for enhanced surface plasmon resonance sensing," *Sci. Rep.*, vol. 8, no. 1, p. 9060, Dec. 2018.

[51] M. A. Otte, B. Sepúlveda, W. Ni, J. P. Juste, L. M. Liz-Marzán, and L. M. Lechuga, "Identification of the optimal spectral region for plasmonic and nanoplasmonic sensing," *ACS Nano*, vol. 4, no. 1, pp. 349–357, Jan. 2010.

[52] H. Jiang and J. Sabarinathan, "Effects of coherent interactions on the sensing characteristics of near-infrared gold nanorings," *J. Phys. Chem. C*, vol. 114, no. 36, pp. 15243–15250, Sep. 2010.

[53] J. Li, J. Ye, C. Chen, Y. Li, N. Verellen, V. V. Moshchalkov, L. Lagae, and P. Van Dorpe, "Revisiting the surface sensitivity of nanoplasmonic biosensors," *ACS Photon.*, vol. 2, no. 3, pp. 425–431, Mar. 2015.

[54] Y. Liang, W. Cui, L. Li, Z. Yu, W. Peng, and T. Xu, "Large-scale plasmonic nanodisk structures for a high sensitivity biosensing platform fabricated by transfer nanoprinting," *Adv. Opt. Mater.*, vol. 7, Apr. 2019, Art. no. 1801269.

[55] M. Vala, C. T. Ertsgaard, N. J. Wittenberg, and S.-H. Oh, "Plasmonic sensing on symmetric nanohole arrays supporting high-Q hybrid modes and reflection geometry," *ACS Sensors*, vol. 4, no. 12, pp. 3265–3274, Dec. 2019.

[56] Y. Liang, Z. Yu, L. Li, and T. Xu, "A self-assembled plasmonic optical fiber nanoprobe for label-free biosensing," *Sci. Rep.*, vol. 9, no. 1, pp. 1–8, Dec. 2019.

[57] N. Nath and A. Chilkoti, "A colorimetric gold nanoparticle sensor to interrogate biomolecular interactions in real time on a surface," *Anal. Chem.*, vol. 74, no. 3, pp. 504–509, Feb. 2002.

[58] Y. Sun and Y. Xia, "Increased sensitivity of surface plasmon resonance of gold nanoshells compared to that of gold solid colloids in response to environmental changes," *Anal. Chem.*, vol. 74, no. 20, pp. 5297–5305, Oct. 2002.

[59] H. Chen, X. Kou, Z. Yang, W. Ni, and J. Wang, "Shape-and size-dependent refractive index sensitivity of gold nanoparticles," *Langmuir*, vol. 24, no. 10, pp. 5233–5237, May 2008.

[60] S. M. Marinakos, S. Chen, and A. Chilkoti, "Plasmonic detection of a model analyte in serum by a gold nanorod sensor," *Anal. Chem.*, vol. 79, no. 14, pp. 5278–5283, Jul. 2007.

[61] N. Liu, T. Weiss, M. Mesch, L. Langguth, U. Eigenthaler, M. Hirscher, C. Sonnichsen, and H. Giessen, "Planar metamaterial analogue of electromagnetically induced transparency for plasmonic sensing," *Nano Lett.*, vol. 10, no. 4, pp. 1103–1107, Apr. 2010.

[62] C. L. Nehl, H. Liao, and J. H. Hafner, "Optical properties of star-shaped gold nanoparticles," *Nano Lett.*, vol. 6, no. 4, pp. 638–688, 2006.
[63] M. A. Mollah and M. S. Islam, "Novel single hole exposed-suspended core localized surface plasmon resonance sensor," *IEEE Sensors J.*, early access, Sep. 14, 2020, doi: 10.1109/JSEN.2020.3023975.
[64] M. S. Islam, M. R. Islam, J. Sultana, A. Dinovitser, B. W.-H. Ng, and D. Abbott, "Exposed-core localized surface plasmon resonance biosensor," *J. Opt. Soc. Amer. B, Opt. Phys.*, vol. 36, no. 8, pp. 2306–2310, 2019.
[65] M. S. Islam, J. Sultana, R. A. Aoni, M. S. Habib, A. Dinovitser, B. W.-H. Ng, and D. Abbott, "Localized surface plasmon resonance biosensor: An improved technique for SERS response intensification," *Opt. Lett.*, vol. 44, no. 5, pp. 1134–1137, 2019.
[66] M. S. Islam, J. Sultana, A. A. Rifat, R. Ahmed, A. Dinovitser, B. W.-H. Ng, H. Ebendorff-Heidepriem, and D. Abbott, "Dual-polarized highly sensitive plasmonic sensor in the visible to near-IR spectrum," *Opt. Exp.*, vol. 26, no. 23, pp. 30347–30361, 2018.
[67] P. Arora, E. Talker, N. Mazurski, and U. Levy, "Dispersion engineering with plasmonic nano structures for enhanced surface plasmon resonance sensing," *Sci. Rep.*, vol. 8, no. 1, pp. 1–9, Dec. 2018.
[68] D. Woolf, M. Loncar, and F. Capasso, "The forces from coupled surface plasmon polaritons in planar waveguides," *Opt. Exp.*, vol. 17, no. 22, pp. 19996–20011, 2009.

AJAY KUMAR AGRAWAL was born in Renukoot, Uttar Pradesh, India, in 1989. He received the B.Tech. degree in electronics and communication engineering from Uttar Pradesh Technical University, Lucknow, India, in 2011, and the M.Tech. degree in opto-electronics and optical communication from IIT Delhi, New Delhi, India, in 2013, where he is currently pursuing the Ph.D. degree with the Electrical Engineering Department.

From 2013 to 2015, he was an Assistant Professor with the Department of Electronics and Communication, Jaypee University of Information Technology, Waknaghat, India. His research interests include SPR- and LSPR-based gas, biological and temperature sensors, photonic integrated devices, plasmonic fiber optic sensors, and flexible electronics and optical devices.

AAKANSHA SUCHITTA received the B.E. degree in electronics and communication engineering from the Netaji Subhas University of Technology, Delhi, India, in 2014, and the M.Tech. degree in radio frequency design and technology from IIT Delhi (IITD), New Delhi, India, in 2016, where she is currently pursuing the Ph.D. degree in electrical engineering with the Prof. Anuj Dhawan's Nanophotonics and Plasmonics Laboratory.

She was a Visiting Scholar with the Birck Nanotechnology Center, Prof. Xianfan Xu's Research Group, Purdue University, IN, USA, from 2019 to 2020. Her research interests include nanophotonics, plasmonics, chiral metasurfaces, optical spectroscopy, chirality detection and biosensors, circuit implementation, and signal processing in electronic devices. She is an Awardee of the Science and Engineering Research Board–Overseas Visiting Doctoral Fellowship (SERB-OVDF) funded by the Government of India.

ANUJ DHAWAN (Member, IEEE) received the B.Tech. degree from IIT Delhi and the M.S. and Ph.D. degrees from North Carolina State University (NCSU), Raleigh, NC, USA.

He has worked as a National Research Council (NRC) Research Associate with the Electronics Division, U.S. Army Research Office (ARO), Durham, NC, USA, from 2007 to 2009, and the Research Scientist of the Fitzpatrick Institute for Photonics, Duke University, NC, USA, from 2009 to 2011. Since 2011, he has been with the Department of Electrical Engineering, IIT Delhi, where he was an Assistant Professor from 2011 to 2016. Since 2017, he has been an Associate Professor with the Department of Electrical Engineering. He leads the Nanophotonics and Plasmonics Research Group as well as the Nanophotonics and Plasmonics Laboratory (NPPL), IIT Delhi. He has authored more than 120 publications (including more than 60 publications in journals of repute), filed several U.S. and Indian patents, and has led several sponsored research projects as a Principal Investigator at IIT Delhi. His research interests include plasmonic and optoelectronic devices, chemical and biological sensors, SPR- and SERS-based sensors, nanofabrication, flexible electronic and photonic devices, integrated nano-scale systems, integrated photonic devices, and computational electromagnetics.